Inventory of supplemental information

Supplemental Figures and Legends

Figure S1 (Related to Figure 1). Procedures for automatic cell identification and calcium traces extraction from GCaMP6s Expressing Neurons.
Figure S2 (Related to Figure 1). Comparison of three difference methods in extracting calcium traces from synthetic data mimicking *in vivo* epi-fluorescent calcium imaging.
Figure S3 (Related to Figure 1). Comparison of performance between CNMF and ARS methods on mouse *in vivo* GCamp6s calcium imaging dataset.
Figure S4 (Related to Figure 2). Details of the clustering analysis of the D1-MSN and D2-MSN *in vivo* GCamp6s calcium imaging dataset.

Movie S1 (Related to Figure 1-2). Simultaneous display of the mouse locomotion, GCaMP6 recording images, and identified neuronal calcium transients for a representative D2-Cre mouse.
Movie S2 (Related to Figure 1-2). Example of automatic cell identification algorithm and calcium traces extraction.

Table S1 (Related to Figure 1-4). Summary of the statistical analysis of the results presented in Figure 1-4 (see attached excel file for details).

Supplemental Experimental Procedures

Supplemental References

Supplemental Figures and Legends

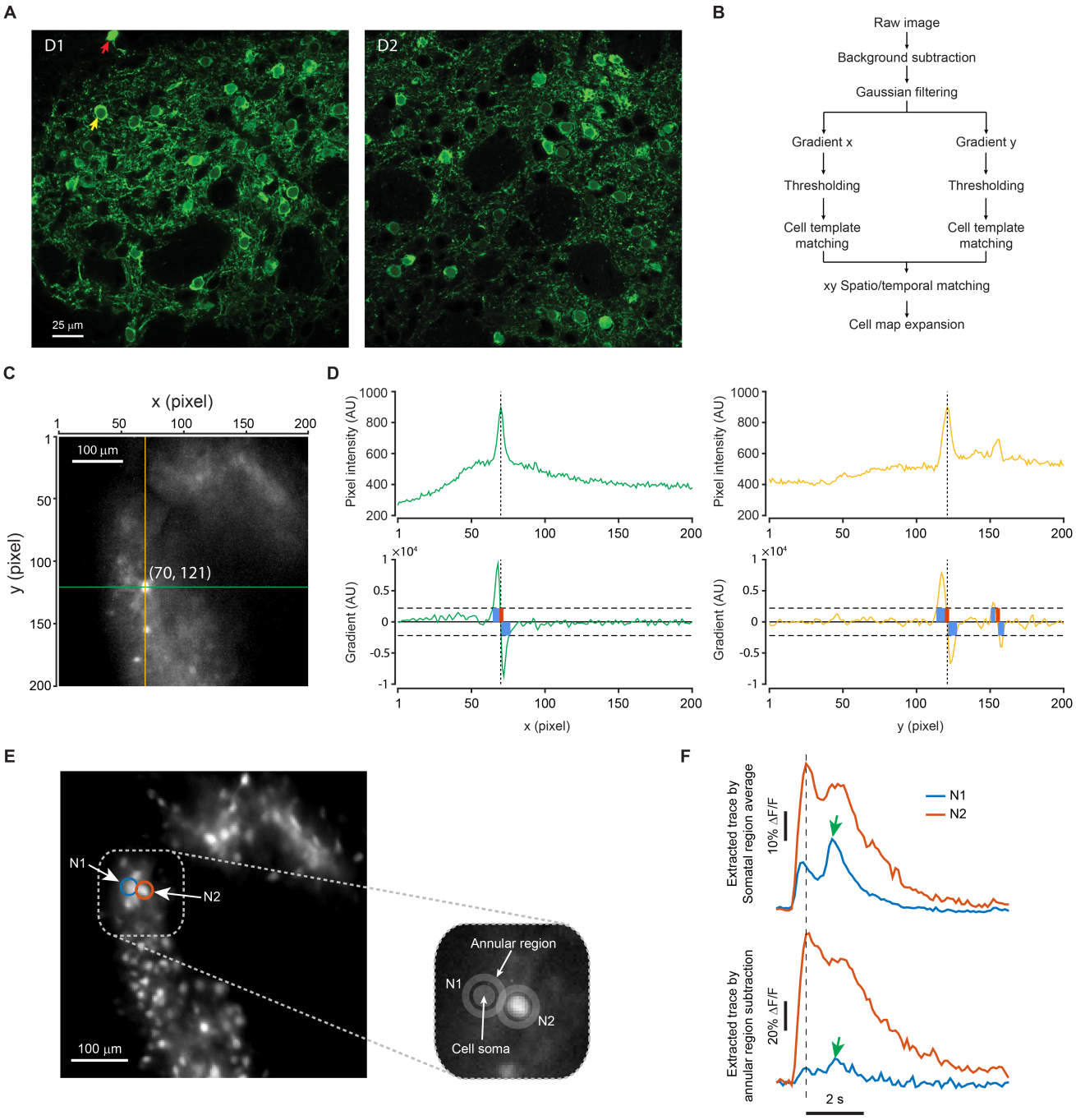

Figure S1. Related to Figure 1. Procedures for automatic cell identification and calcium traces extraction from GCaMP6s Expressing Neurons. A. Representative confocal images (Zeiss LSM 710; 63× objective; 255μm×255μm) from brain slices of D1-Cre mouse (Left panel) or D2-Cre mouse (Right panel) injected with AAV1.CAG.Flex.GCaMP6s.WPRE.SV40, 2 months after AAV injection. A total of 97.6 % ± 0.9% (mean ± s.e.m.) of neurons showed nuclear exclusion of GCaMP6s (n = 8 brain slices from eight mice), indicating that both D1- and D2- MSN were in good health after 2 month of GCaMP6 expression. Yellow arrow indicated an example of nuclear exclusion of GCaMP6 in healthy neuron. Red arrow indicated an example of nuclear filling of GCaMP6 in unhealthy neuron. Scale bar, 25 μm. **B.** A diagram of the Spatio-Temporal Gradient Matching (STGM) cell identification algorithm workflow: after background subtraction and 5x5 Gaussian filtering, the x and y gradients of the pixel intensity were independently calculated (Gradient X and Gradient Y), a threshold was then applied (Thresholding), then matched to a typical cell template (Cell template matching); if the match was positive in the same location for both the x- and y- gradient (xy spatio-matching) for a minimum of 3 consecutive frames (temporal-matching), a new cell was added to the overall cell map (Cell map expansion).

See **Supplemental Experimental Procedures** for more detail in cell identification. **C.** A representative background subtracted image of a frame showing the position of a candidate cell at the cross-point of the horizontal and vertical lines. For any given line, fluorescent value along the line is expressed as F(x, y). Therefore, the horizontal x line shown in **C** is expressed as F(x, 121) for y=121; the vertical line shown in **C** is expressed as F(70, y) for x=70. The cross point of line x and y is expressed as F(70, 121). **D.** Pixel intensities (top traces) and gradient (bottom traces) for the horizontal line (left panels, F(x, 121), green line in **C**) and vertical line (right panels, F(70, y), yellow line in **C**). Cell centroid F(70, 121) (cross point of green and yellow lines in **C**) were identified by a sequence of positive and negative peaks in the gradient trace (lower panels, blue shaded areas). The cell was added to the cell map if its centroid was detected at the same location (F(70, 121)) both in x gradient (F(x, 121)) and in y gradient (F(70,y)) for 3 consecutive frames (spatio-temporal matching). **E.** Two identified neurons were highlighted in an image stack projection of standard deviation (to give the overall intensity map of the neurons). Blue circle indicated neuron N1 and orange circle indicates neuron N2. Inset showed a zoom-in view of N1 and N2 neuron area (time point corresponding to the time indicated by the dash line in b). In the inset panel, the soma ROI (gray filled circle) and contamination background region (gray annular ring) were shown for N1 and N2. **F.** Traces showing the resulting calcium transients from ROI before (top panel) and after (bottom panel) removing the contamination fluorescent activity within the annular region. The contamination signal (green arrow) were removed after the annular background subtraction. See **Supplementary Experimental Procedures** for more details.

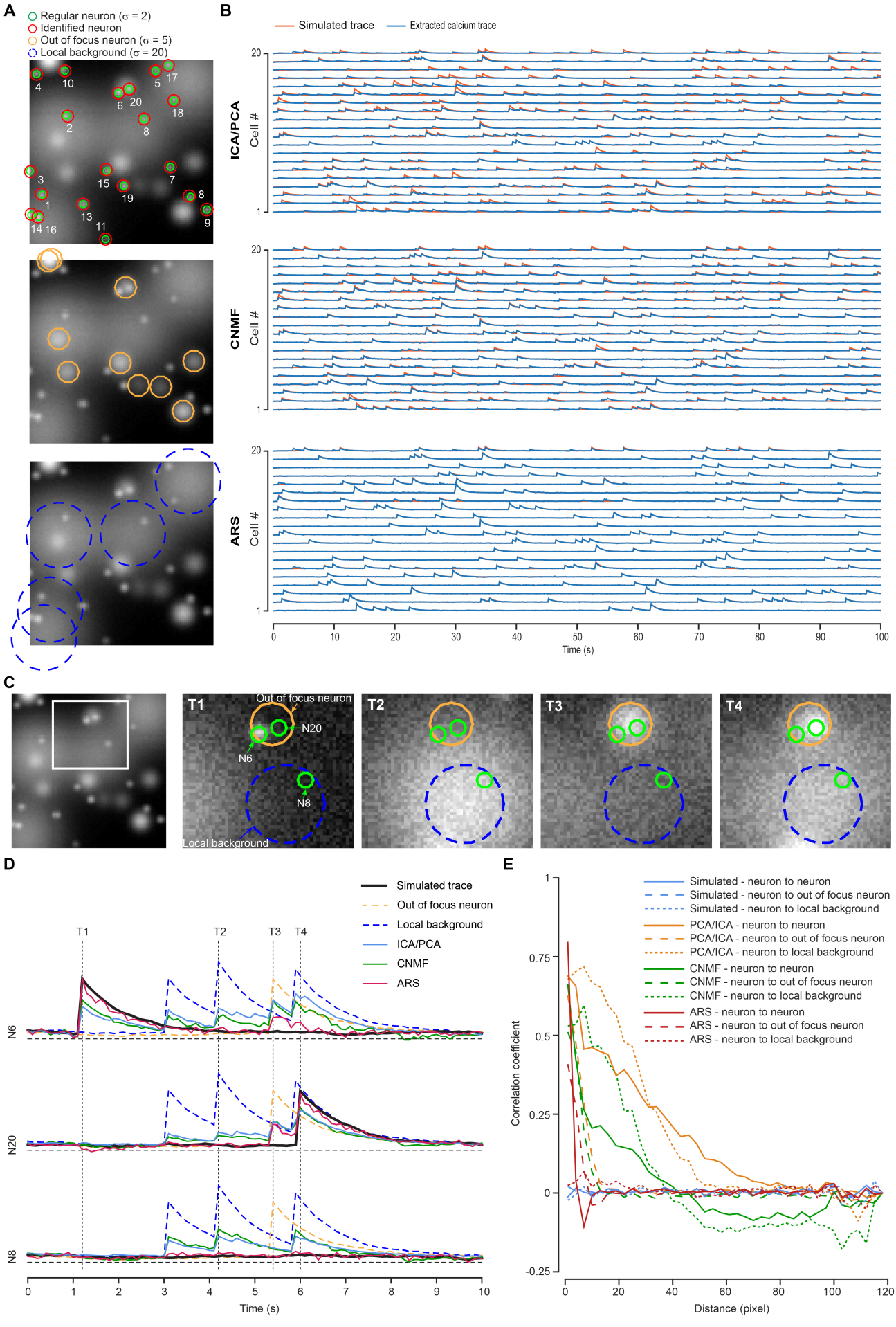
A
Regular neuron (σ = 2)
Identified neuron
Out of focus neuron (σ = 5)
Local background (σ = 20)
B
Simulated trace
Extracted calcium trace
ICA/PCA
CNMF
ARS
Cell #
Time (s)
C
T1
T2
T3
T4
Out of focus neuron
N20
N6
N8
Local background
D
Simulated trace
Out of focus neuron
Local background
ICA/PCA
CNMF
ARS
N6
N20
N8
Time (s)
E
Simulated - neuron to neuron
Simulated - neuron to out of focus neuron
Simulated - neuron to local background
PCA/ICA - neuron to neuron
PCA/ICA - neuron to out of focus neuron
PCA/ICA - neuron to local background
CNMF - neuron to neuron
CNMF - neuron to out of focus neuron
CNMF - neuron to local background
ARS - neuron to neuron
ARS - neuron to out of focus neuron
ARS - neuron to local background
Correlation coefficient
Distance (pixel)

Figure S2. Related to Figure 1. Comparison of three difference methods in extracting calcium traces from synthetic data mimicking in vivo epi-fluorescent calcium imaging. A. Representative standard deviation projection images for a 100-second simulated experiment, with highlighted position for three different types of simulated signals: in-focus neurons (green circles, top panel), out-of-focus neurons (orange circles, middle panel) and local background regions (blue dashed circles, bottom panel); Red circles in the top panel indicated the location of all neurons identified by the proposed gradient based Spatio-Temporal Gradient Matching (STGM) cell identification algorithm, showing that the STGM algorithm correctly identified all simulated in-focus neurons while eliminated out-of-focus neurons. **B.** Comparison of the actual simulated calcium traces with extracted fluorescent traces using PCA/ICA (principal component analysis / Independent Component Analysis; top panel), CNMF (middle panel) and the Annular Region Subtraction method (ARS) used in this work (bottom). Red traces on each panel indicate actual simulated calcium traces (ground truth), and blue traces indicate calcium traces extracted using method as indicated. This result suggests that ARS can reliably extract fluorescent traces from the synthetic dataset. **C.** Representative standard deviation projection image for a 100-second simulated experiment (top panel), and high magnification images from boxed area at 4 different time instants (T1 through T4). Boxed area contained three in-focus neurons (green circles, N6, N8, and N20), one out-of-focus neuron (orange circle), and one local background region (blue dashed circle). **D.** Comparison of extracted calcium traces of N6, N8 and N20 in a 10-second time window using different methods. In the actual simulation data (black traces), N6 and N20 displayed one peak activity at T1 and T2, respectively; but N8 displayed no calcium activity (being silent) in the considered 10-second time window. All three methods: PCA/ICA (cyan traces), CNMF (green traces), and ARS (red traces), were able to efficiently separate calcium transients of the three neighboring neurons (green circles in **C**), with no appreciable cross talk. However, the calcium activity from the nearby out-of-focus neuron (dashed orange traces) and local background (dashed blue traces) had substantial effects on the calcium traces calculated with the PCA/ICA (cyan traces) and CNMF (green traces) methods, leading to false activity peaks for N8. By contrast, the ARS method was able to correctly identify the lack of activity of N8 during the indicated 10-second period (note: N8 was identified using the 100-second simulated data and has activity outside of this 10-second time window). **E.** Average inter-neuron Pearson's correlation coefficient as a function of distance for the three types of signals considered (bin size 3 pixel): in-focus neurons (N), out-of-focus neurons (O), and local background fluorescent flashes (B). In the simulated data set (blue traces), we set the correlation between N to N, N to O, and N to B to zero. All three methods were able to greatly reduce neuron and out of focus neuron (N to O) correlation to a similar degree (Orange, Green, and Red dashed traces). But PCA/ICA does not perform as well in reducing correlation with nearby neurons (N to N) and local background regions (N to B). Better performance in terms reducing N to N correlation was achieved with CNMF, but N to B correlation could not be efficiently reduced using CNMF. The ARS method used in this paper to extract calcium fluorescent traces further reduced N to N compared to CNMF, and reduced N to B to zero, indicating efficient elimination of local background fluorescent flashes from our final calcium traces. These results suggest that our ARS method is at least as good as CNMF in extracting fluorescent traces, and that both ARS and CNMF performed better than PCA/ICA.

Details of the application of PCA/ICA, CNMF to the synthetic data:
PCA/ICA: Cell sort algorithm (PCA/ICA) was used based on previous study (Mukamel et al., 2009). The PCA was first used for data dimensionality reduction. Usually 50 principal components (PC) were compute for the dataset. The high boundary number for the PC was chosen roughly based on the converging point of the slopes of the signal and noise spectra. The low boundary number was set around 12. Then the ICA was used to obtain the spatial filters. The number of independent components (ICs) was chosen between 16 to 25 based on the number of the neurons. Further steps including ROI separation and ROI selection were performed to obtain spatial filters for the in-focus neurons. Calcium traces ($\Delta F/F$) were then extracted and compared with the synthetic data (ground truth).
CNMF: The recent published CNMF method by Pnevmatikakis and colleagues was used (Pnevmatikakis et al., 2016). To simplify the calculation, the true positions of the 20 in-focus neurons were used as the input of the greedy initialization algorithm. The size of the filter kernel was set to 3×3 and window of 6×6. The autoregressive (AR) order was chosen to be 1 since our imaging frame rate is 10Hz, as suggested by the authors (Pnevmatikakis et al., 2016), and the ROI merging was applied with a threshold of 0.8. Lastly, the calcium traces ($\Delta F/F$) were calculated and compared with the synthetic data (ground truth).

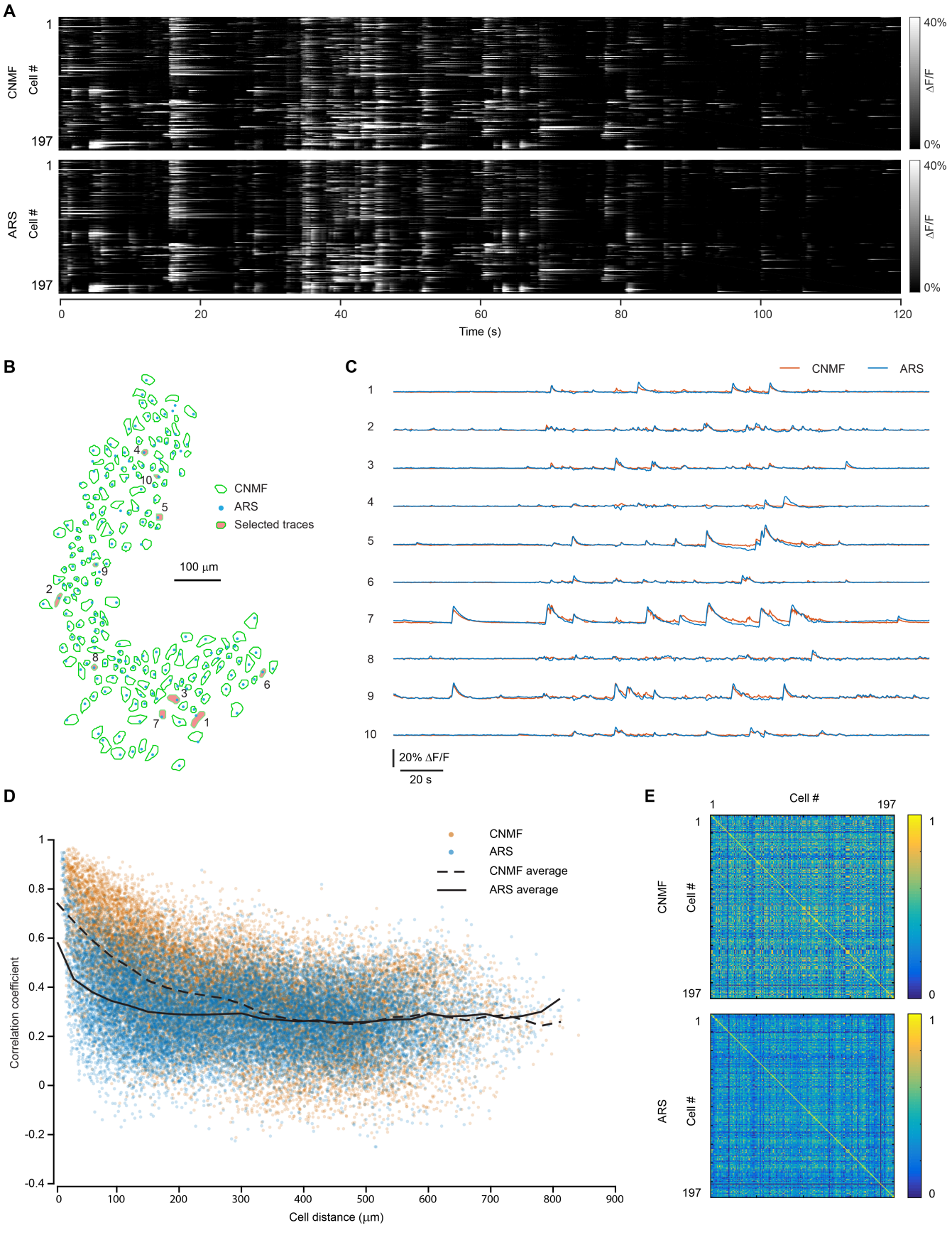
A
CNMF
Cell #
1
197
ARS
Cell #
1
197
40%
ΔF/F
0%
0
20
40
60
80
100
120
Time (s)
B
CNMF
ARS
Selected traces
100 μm
C
CNMF
ARS
20% ΔF/F
20 s
D
CNMF
ARS
CNMF average
ARS average
Correlation coefficient
Cell distance (μm)
E
Cell #
CNMF
ARS

Figure S3. Related to Figure 1. Comparison of performance between CNMF and ARS methods on mouse *in vivo* GCamp6s calcium imaging dataset. A. Representative raster plots showing high degree of similarity between the calcium traces for a D2-Cre mouse in vivo recording, extracted with CNMF (top panel) and with ARS (bottom panel). **B.** Comparison of cell map identified using CNMF and our Spatio-Temporal Gradient Matching (STGM) algorithm. Green mask contours indicated neurons identified using the CNMF framework, blue dots indicated cell centroid identified using our spatio-temporal gradient matching method. This result demonstrated that our STGM method and CNMF framework identified majority of neurons at the same location and the overall cell map were almost identical. **C.** Comparison of calcium traces extracted using CNMF and ARS showed similar results. The 10 representative neurons were distributed throughout the cell map (marked in red on the cell map shown in **B**. **D.** Inter-neuron correlation coefficient as a function of cell distance. ARS method showed a slightly better decoupling of neighboring neurons than CNMF. **E.** Pearson's correlation matrix of the calcium traces calculated with CNMF (top) and with the ARS method (bottom). Neuron pairs from CNMF extraction method displayed a slightly higher correlated activity than ARS, demonstrating that ARS method offered a more efficient decoupling of neural activity in spatially adjacent neurons.

Details of the application of CNMF to a representative D2 data: the identified positions from our gradient based cell identification algorithm was used as the input of the greedy initialization algorithm. The size of the filter kernel was set to 3x3 and window of 6x6. The autoregressive (AR) order was chosen to be 2 as suggested by the report since our imaging frame rate is 10Hz. And a merging threshold of 0.8 was applied. Lastly, the calcium traces were calculated for the comparison.

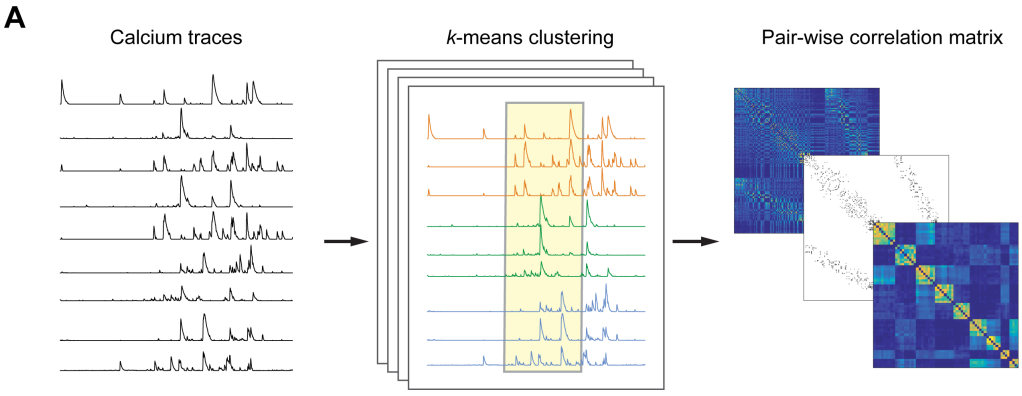

B

Clustering algorithm

for $i = 1{:}1000$ **do**
  Select sample from dataset
  for $j = 1{:}100$ **do**
    Initialize cluster centroids $\boldsymbol{\mu}_k$ with k-means++
    repeat
      Assign elements to closest cluster:
      $\mathbf{c}_i = \{j : d(\boldsymbol{x}_j, \boldsymbol{\mu}_i) \leq d(\boldsymbol{x}_j, \boldsymbol{\mu}_l), l \neq i, j = 1, \ldots, N\}$
      Update cluster centroids:
      $\boldsymbol{\mu}_i = \frac{1}{|\mathbf{c}_i|} \sum_{j \in \mathbf{c}_i} \boldsymbol{x}_j, \forall i$
    until Convergence
  end for
end for
Generate co-occurence matrix
Calculate optimal threshold T and generate meta clusters

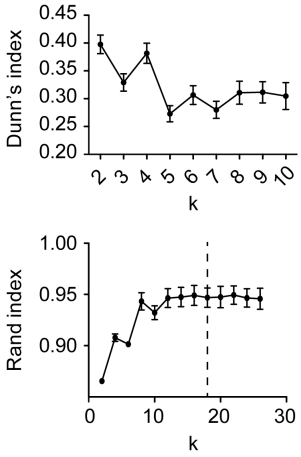

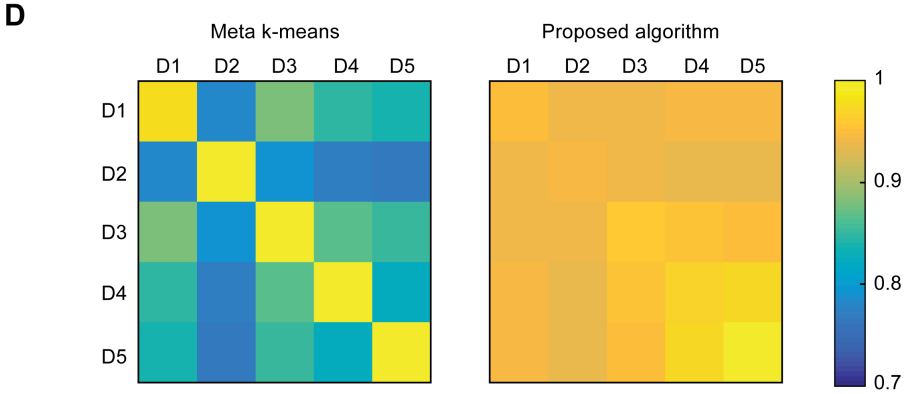

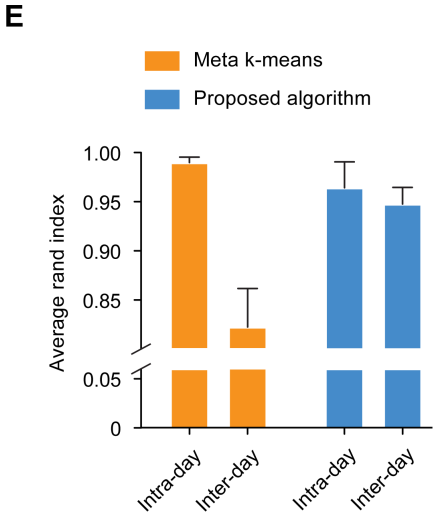

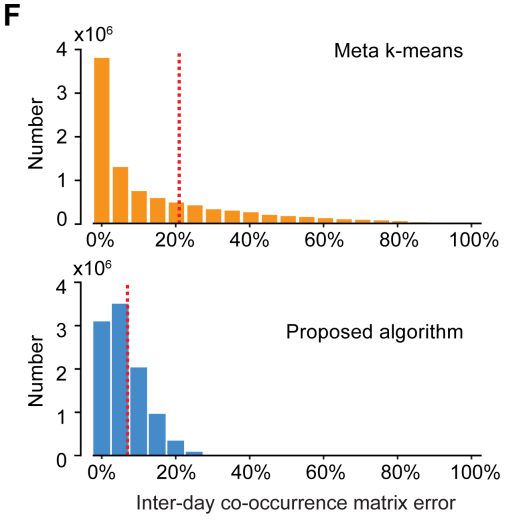

Figure S4. Related to Figure 2. Details of the clustering analysis of the D1-MSN and D2-MSN in vivo GCamp6s calcium imaging dataset. A. Steps for neural cluster analysis: calcium traces (left panel) were grouped based on their activity correlation based on K-means clustering (middle panel), and final cluster was performed using meta-cluster analysis based on pair-wise correlation between any pair of neurons (See **Supplementary Experimental Procedures** for details). **B.** Pseudo-code of the k-means based cell clustering algorithm. **C.** Top panel. An example of the average Dunn's index as a function of k: the peak in the Dunn's index is typically used to find the value of k to use in the k-means algorithm to best describe the dataset, but in this case it fails to provide a reliable estimate. Bottom panel. Average Rand index of the final clustering schemes for different values of k: for low values of k the final clustering can be quite different from trial to trial, but a plateau is reached where the final outcome of the clustering algorithm is consistent within different trials. In our calculations we used the square root of the total number of neurons (dashed line in the figure) as the optimal k. **D.** Mean Rand index for different runs of the clustering algorithm within the same dataset (diagonal terms) and across 5 different days (off-diagonal terms). Rand index is a measure of classification quality between two clustering methods, and expresses the ratio between all pairs of elements placed in both cases in the same cluster or in different clusters over all possible pairings. Despite the high indices within the same dataset, the meta k-means algorithm has poor consistency across different sessions, indicating that it can capture dataset-specific functional features of the neurons, but it fails to group cells according to a more general statistical description of the calcium traces. **E.** Direct comparison of the mean intra-dataset and inter-dataset Rand indices, showing a significant improvement in the overall consistency of the final clustering structure. **F.** Histogram showing the distribution of the average inter-dataset absolute difference in the co-occurrence matrix elements for the meta k-means (top) and the proposed algorithm (bottom): the long tail in the meta k-means variation distribution, which indicates significant differences in the individual partitioning schemes, is considerably reduced in the proposed algorithm. Five datasets were considered for 5 different days, and the mean absolute variance (dotted red line) was 20.48% for the meta k-means and 7.31% for the proposed clustering algorithm.

Movie S1
Simultaneous display of the mouse locomotion, GCaMP6 recording images, and identified neuronal calcium transients for a representative D2-Cre mouse.
Section 1.
Left Panel: A freely moving mouse with a head-mounted miniScope in an open field. The centroid of the mouse was tracked and shown as a green dot. The green line indicates the trajectory of the mouse locomotion. Text on northwest shows time stamps. Scale bar: 3 cm. The red histogram bar indicates the locomotion velocity of the mouse.
Middle Panel: GCaMP6 calcium images from miniScope during mouse locomotion. Scale bar: 100 μm. Right Panel: Calcium transients of the neurons identified in the field of view in a 20-s time window. The x-axis indicates time in seconds, and each line on the Y-axis indicates calcium transient for one neuron.
Section 2.
Left Panel: A freely moving mouse with a head-mounted miniScope in an open field, details same as described in Section 1.
Middle Panel: GCaMP6 calcium images from miniScope during the mouse locomotion. Green dots indicate the centroids of the neurons identified in the field of view (Cell map; Neurons stay active for 5 days). Red dots show the centroids of active neurons among the cell map during the mouse locomotion. Scale bar: 100 μm.
Right Panel: Same as described in Section 1.

Movie S2
Example of automatic cell identification algorithm and calcium traces extraction.
Section 1.
Application of the automatic gradient based cell identification algorithm for a representative D2-Cre mouse: GCaMP6 calcium images from miniScope during locomotion. The neural map updated at each timestep is overlayed in green. Scale bar: 100 μm.
Section 2.
Calcium traces extraction for a representative D2-Cre mouse:
Left panel: GCaMP6 calcium images from miniScope during locomotion; 6 neurons are randomly selected from a densely populated region.
Right panel: Calcium traces extracted with the Annular Ring Subtraction method for the six neurons highlighted in the right panel. Despite the proximity of the neurons with each other, their calcium traces do not show appreciable correlation.

Table S1 Summary of the statistical analysis of the results presented in Figure 1-4 (see attached excel file for details).

Supplemental Experimental Procedures

Design of Miniature Epifluorescence Microscope

A custom-built miniature epifluorescence microscope (miniScope) was used to image GCaMP6 fluorescence. The miniScope has a 2.4-gram weight and approximately 1.1 mm×1.1 mm maximum field of view with a cellular spatial resolution.

Optics: A 3.5 mm×3.5 mm blue LED (XLamp XP-E, Cree) with 465 nm peak wavelength was used as the excitation light source. The illumination light was collimated using a 4-mm diameter, 2.73-mm focal length aspherical lens (#83-605, Edmund optics), passing through a 3 mm×3 mm square excitation filter (ET470/40, Chroma Technology), and was reflected by a 5 mm×5 mm dichroic mirror (FF495, Semrock) with a cutoff wavelength of 495 nm. Another 4-mm diameter aspherical lens (#83-605, Edmund optics) was used as an objective lens to collect fluorescence originated from dorsal striatum and relayed via the GRIN lens. The fluorescence emission passed through the dichroic mirror and emission filter (EM525/50, Chroma Technology), and was focused by a 4-mm diameter 6-mm focal length achromatic doublet lens (#63-690, Edmund optics), to form the fluorescent image on a complementary metal-oxide semiconductor (CMOS) sensor (MT9V022IA7ATM, Aptina). The distance between objective lens and imaging lens was optimized using optical design software ZEMAX (Zemax).

Mechanical Design: Solidworks (Dassault Systèmes) was used for mechanical design of the microscope parts. Stereolithography technique (Proto Labs) was used for 3D printing of the miniScope housing. The material was SLArmor Nickel-NanoTool (Proto Labs) that is ultra-stiff, lightweight and light-tight. The miniScope consists of a main body, a filter cube, and a base. The main body and the base were connected using 0.5-mm pitch thread, which allows for focus adjustment within ~2.0 mm range. A side locking screw on the base was designed for locking the in-focus position of the miniScope body. The height of the base was designed taking into consideration of both the height of GRIN lens on the top of the skull and the working distance of the miniScope.

Data Acquisition System: The data acquisition system was built based on a field-programmable gate array (FPGA; XEM3001v2, Opal Kelly). The FPGA was used to control the CMOS image sensor and the microscope excitation LED. A custom control program was developed in C++ to communicate with the FPGA board from PC through a USB port. The imaging sensor was integrated into a small lightweight PCB board containing all the components to transmit the acquired images through low-voltage differential signaling (LVDS) serial interface. The size of the entire imaging PCB is 11 mm×10 mm×6 mm. A custom built cable was used to connect the sensor and data acquisition system. The cable consists of a slip ring and a 12-wire bundle. The frame rate for calcium imaging was 10 Hz with a 400×400 pixels image covering a 1.1 mm×1.1 mm field of view. The time stamps were recorded for synchronization with the behavioral video recording system.

Animal Use

All experiments were conducted in accordance with the guidelines of Institutional Animal Care and Use Committee, the Intramural Research Program, National Institute on Drug Abuse, National Institutes of Health. Transgenic mice expressing Cre recombinase under the control of the dopamine D1 receptor (D1-Cre, FK150 line, C57BL/6J congenic, Gensat, RRID:MMRRC_036916-UCD) or dopamine D2 receptor (D2-Cre, ER44 line, C57BL/6J congenic, Gensat, RRID:MMRRC_032108-UCD) were used in the experiments. All mice were male at 3-4 months of age and 25-30 gram of weight. All mice were maintained in a regular light cycle (7:00am – 7:00pm) and provided with food and water ad libitum.

Viral Injection

To image GCaMP6 fluorescence in dorsal striatum (DS), we first injected AAV1.CAG.Flex.GCaMP6s.WPRE.SV40 (University of Pennsylvania Vector Core) into the dorsal striatum. The AAV viruses were injected using the stereotactic coordinates (A/P: -0.93 mm, M/L: +1.8 mm, D/V: -3.46 mm, with 30° angle shift to caudate). Mice were anaesthetized with 2 % isoflurane in oxygen at a flow rate of 0.4 liter/min and mounted on a stereotactic frame (Model 962, David Kopf Instruments). Mice body temperature was maintained at 37 °C using a temperature control system (TCAT-2DF, Physitemp). Sterile ocular lubricant ointment (Dechra Veterinary Products) was applied to mouse corneas to prevent drying. Mouse scalp fur was shaved and mouse skin was cleaned with 7.5% betadine and 70 % alcohol. A hole was drilled at the injection site (A/P: -0.93 mm; M/L: +1.8 mm) using a 0.5-mm diameter round burr on a high-speed rotary micro drill (19007-05, Fine Science Tools). A total of 500 nl of virus solution was injected at a rate of 25 nl/min using a micro pump and Micro4 controller (World Precision Instruments). After the injections, the injection needle was kept in the parenchyma for 5 min before being slowly withdrawn. The hole on the skull was then sealed with bone wax, and skin was sutured. Mice were returned to their home cage to recover from anesthesia in a 37 °C isothermal chamber (Lyon Technologies, Inc).

GRIN Lens Implantation

One week after viral injection, a 1-mm diameter gradient index (GRIN) lens (GRINTECH GmBH) was directly implanted in the mouse brain right above the dorsal striatum under anesthesia with ketamine/xylazine (ketamine:100mg/kg. xylazine:15mg/kg). In brief, a 1.1mm-diameter craniotomy was made at the coordinates(A/P:+0.9mm. M/L:+1.8mm). The brain tissue above the dorsal striatum was precisely removed using vacuum through a 30-Gauge blunted needle attached on a motorized stereotactic instrument, which was a custom-constructed three-axis motorized translation stage (MTS50Z8, Thorlabs). MATLAB-based software was developed to control the movement of the stereotactic arm to remove the brain tissue automatically by pre-defined trajectory guidance. The GRIN lens above the mouse skull was secured to skull with dental cement (DuraLay) and an additional plastic cap (0.2-mL PCR tube tip) was glued (Loctite) on the skull to protect the imaging surface of the GRIN lens.

GCaMP6 Imaging in Freely Moving Mice

Two weeks after the GRIN lens implantation, the miniScope base was mounted onto the mouse head. The motorized stereotactic instrument was used to hold the miniScope (including main body and base). After achieving the in-focus position for the entire field of view, the base was fixed on the skull using dental cement. This way, we could attach the miniScope body to mouse head before each experiment and detach it from mouse head after each experiment.

Behavioral Tests

We conducted a 5-day open-field test with a 34 cm×40 cm×20 cm chamber for all D1-Cre and D2-Cre mice. All the behavior tests were done in the light cycle. The top view of mice locomotion was recorded using a custom video camera controlled by custom software in C++, and the start of the recording was triggered by the start of calcium imaging. Similarly, the time stamps were also recorded for the synchronization between the locomotor behavior and the calcium imaging recording. Mice were anesthetized briefly using isoflurane before the miniScope was mounted. We then waited 25 minutes for mice to recover before the first imaging session. For each strain of mice, we included a cocaine-injected group as the experimental group and a saline-injected group as the control group; the cocaine dose was 20 mg/kg, i.p, the injection volume was 10 ml/kg, and cocaine was dissolved in saline. On each day of recording, we first acquired three sessions of 5-minute simultaneous recording for GCaMP6s fluorescent signal and mouse behavior. A 5-minute resting period was incorporated between two consecutive sessions. After three sessions, we injected mice with either cocaine or saline, and waited for two minutes to avoid injection stress. We then acquired calcium recordings for three more 5-minute sessions, with 5-minute resting period incorporated between two consecutive imaging sessions. The entire experiment on each day lasted approximately one hour per mouse.

Calcium Images Analysis

The calcium images were processed and analyzed using custom scripts in MATLAB.

Image Registration: Raw images for each experiment were stabilized with a Fourier-based phase correlation image registration algorithm (Kuglin, 1975) to compensate for the brain translations caused by mouse movements.

Neuron Identification: A gradient-based automatic cell detection algorithm (Lindeberg, 1998), the Spatio-Temporal Gradient Matching (STGM) method, was used to iteratively generate a cell map (centroids for each and all active neurons) for each session frame by frame (**Figure S1**). Background subtraction was firstly applied for the image stack of each session. Images were then smoothed through convolution with Gaussian kernel of 3×3 pixels standard deviation. Next, the x and y gradients (G_x and G_y) of the smoothed image I_{xy} were independently calculated by $G_x = \partial I_{xy}/\partial x$, and $G_y = \partial I_{xy}/\partial y$. A threshold was then applied to G_x and G_y as the following:

$$G_x = \begin{cases} sign(G_x) & if\ |G_x| \geq T_x \\ 0 & if\ |G_x| < T_x \end{cases} \qquad G_y = \begin{cases} sign(G_y) & if\ |G_y| \geq T_y \\ 0 & if\ |G_y| < T_y \end{cases},$$

where the thresholds T_x and T_y are set to 4 times the root mean square (RMS) of G_x and G_y, respectively. Subsequently, a simple template matching algorithm was applied to detect all sequences of positive and negative gradient peaks (indicating the edges of in-focus neurons) within a maximum distance D = 30 μm (12 pixels). If the template was matched at the same x-y location for both G_x and G_y for 3 consecutive frames, a 2×2 pixel mask was added as a new cell to the overall cell map of the current recording session. Finally, for each session, the cumulative cell map was segmented, and each cell's location was calculated as the centroid of each segmented region. An example of the application of the automatic cell identification algorithm is shown in **Movie S2**.

Alignment of cells across different days of imaging: For the alignment of images from recording sessions across different days we used standard methods similar to other previous studies (Pinto and Dan, 2015; Ziv et al., 2013) to adjust and

compensate for the image translation rotation and dilation caused by repositioning of the microscope. After the day-to-day registration, an overall cell map was generated by merging the 5 day cell map. To confirm the performance of the neuron identification, visual inspection was conducted by overlaying the cell map on the calcium images.

Calcium traces calculation: The calcium traces were extracted using the Annular Region Subtraction (ARS) method for each identified neuron through the following procedure (Also see **Figure S1**): first a neuron ROI (region of interest) was assigned as a circular region corresponding to the size of soma (diameter = 15 μm) of D1 and D2 neurons with the centroid as detected. The image stack minimum F_0 was used as the baseline fluorescence of the background. The ROI fluorescence F_{ROI} was calculated as the maximum fluorescence value of the background subtracted images over the ROI, $F_{ROI} = \max(F_{Raw} - F_0)_{ROI}$, where F_{raw} is the raw image. Next, a commonly used formula (Chen et al., 2013b; Kerlin et al., 2010; Pinto and Dan, 2015) was applied to correct the potential contamination from out-of-focus neurons or/and neuropil fluorescence, i.e. $F_{sig} = F_{ROI} - \gamma F_{con}$ where F_{sig} is the true fluorescence signal, F_{con} is contamination fluorescence and was calculated as the minimum value of the background subtracted images over an annular region (d_1 = 20 μm, d_2 = 30 μm) surrounding the soma ROI ($F_{con} = \min(F_{raw} - F_0)_{annular}$), and γ is the contamination factor, empirically estimated by the ratio of fluorescence in blood vessel region and fluorescence in the annular region. The values of γ in this study ranged from 0.57 to 0.99 (mean ± s.e.m.: 0.88 ± 0.02; n = 18 from 6 mice), which are higher than other studies using two-photon calcium imaging. This is due to higher contamination from out of focus fluorescence in epi-fluorescence microscopy used in the current study as opposed to two-photon microscopy. In our final calculation, $\gamma = 1$ was used to minimize the effects of the contamination fluorescent signals. Consequently, each calcium trace $\Delta F/F$ was calculated as F_{sig}/F_b, where $F_b = \langle F_0 \rangle_{ROI}$ is the baseline fluorescence over the soma ROI. The binary rasterplots used in some of the data analyses were generated by applying a threshold of three times the root mean square (RMS) of each neuron's baseline fluorescence. Calcium transient onset was defined as $\Delta F/F$ crossing the threshold of three times the RMS of the calcium trace baseline. For each calcium transient, the local maxima (3s window from transient onset) was identified, and the amplitude and time decay constant can be estimated by fitting the transient decay data (3 s window from the local maxima) with an exponential function $A\exp(-t/\tau_0)$, where A is the amplitude and τ_0 is the time decay constant.

Detailed procedure for the generation of synthetic data: In a field of view of 100 × 100 pixels, three types of Gaussian shaped signals were placed: 20 regular cells (standard deviation $\sigma_1 = 2$ pixels, based on average measured cell size) representing the in-focus neurons, 10 out-of-focus cells (standard deviation $\sigma_2 = 5$ pixels) simulating the blurry neurons and the spillover effects from the neurons with high intensity of activations (Ziv et al., 2013), and 5 large regions (standard deviation $\sigma_3 = 20$ pixels), simulating the activation of large out-of-focus neuronal populations or neuropils (**Figure S2A**). The position of the centroid of each signal was chosen with uniform distribution across the field of view. Under the simplified assumption that the fluorescent trace is a linear observation of the calcium concentration $[CA^{2+}]$ (Vogelstein et al., 2009), the underlying spike trains were generated from a Bernoulli process with probability $\lambda = 0.001$. The calcium concentration was then calculated according to the model (Vogelstein et al., 2009):

$$[CA^{2+}]_t - [CA^{2+}]_{t-1} = -\frac{T_c}{\tau}([CA^{2+}]_{t-1} - [CA^{2+}]_b) + An_t + \sigma_c \varepsilon_{c,t}\sqrt{T_c}$$

where T_c is the sampling period for calcium imaging, τ is the exponential decay time constant, $[CA^{2+}]b$ is the calcium concentration bias, A is a proportional constant, n_t is the total number of spikes during the t-th frame, and $\sigma_c\varepsilon_{c,t}\sqrt{}Tc$ is the noise of the calcium concentration model scaled with the time period T_c. To evaluate the performance of the proposed algorithm for a wide spectrum of SNR (signal to noise ratio), the single pixel signal was corrupted with Gaussian noise of standard deviation $\sigma_p = 0.01, 0.05, 0.1, 0.3, 0.5$ and 1, respectively; five simulations were run with different initial cell positions for each value of σ_p. Details of the application of calcium analysis methods to the synthetic data are shown in **Figure S2**.

Neural Clustering Analysis

Clusters of neurons were identified based solely on their neural activity information (ΔF/F), through a clustering algorithm based on the meta k-means algorithm (Ozden et al., 2008) and outlined in **Figure S4**. The similarity metric chosen for the cluster assignment was the Pearson's correlation coefficient. The basic k-means algorithm with k-means++ seeding (Arther, 2007) was run 100 times on each of 1000 randomly sampled 30 s subsequences. For the choice of k, the use of Dunn's index (Dombeck et al., 2009) could not provide useful information in our dataset due to the lack of a clear peak (**Figure S4C**, top panel). Instead we found that by using the square root of the number of neurons in the field of view (a common approach in literature (Pham, 2005) when no a priori information about the clustering scheme is available) yields consistent results in terms of reiteration of the clustering algorithm on the same dataset (**Figure S4C**, bottom panel). Rand index (Rand, 1971) is used here as a similarity metric to compare two different clustering schemes, ranging from 0 (no pair of elements are clustered together in both clustering schemes) to 1 (the two clustering schemes are identical). Based on the outcome of this iterative clustering step, we generated a pairwise co-occurrence matrix containing on each entry (i, j) the number of times that cells i and j are clustered together. The final clusters were defined as the largest sets of cells clustered together at least T times. This threshold T was chosen to maximize the ratio between number of final clusters and number of unclustered cells.

The proposed clustering method substantially improves the consistency of the meta k-means algorithm outcome across different imaging sessions (**Figure S4**).

Intra-cluster pairwise cell distance was defined as the average of all pairwise cell distances in each cluster. The centroid of cluster was defined as the average centroid of all neurons in this cluster. Intra-cluster pairwise correlation coefficient was defined as the average of all pairwise Pearson's correlation coefficients of neurons in each cluster. The neightboring (or adjacent) cluster pairwise correlation coefficient for cluster A was defined as the average of all pairwise Pearson's correlation coefficients of neurons in cluster A with the neurons in nearest cluster B (minimum cluster centroid to centroid distance). The spatical distubution of neurons in each cluster can be estimated by Parzen probability density estimation method with a Gaussian kernel (Duda et al., 2000). Thus a smoothed contour of each cluster was estimated.

Activity Synchronization Analysis

Each calcium transient onset was identified with the threshold crossing of three times the RMS of the calcium trace baseline, and a binary matrix of the calcium transient onsets for all cells was created. In order to compensate for the ±1 frame uncertainty in the threshold crossing detection, each event is represented in the binary sequence as a 300 ms (3 frames) pulse centered at the calcium transient onset. In pairwise cell analysis, two events are considered to be synchronous if they overlap during at least one time instant. We then calculated the asymmetric correlation coefficient (Schwartz et al., 1998), defined for any pair of cells (i, j) as the ratio of the times both cells are simultaneously active over the total activations of cell i. The asymmetric correlation coefficients were calculated for each daily imaging session (before and after i.p injection) and averaged over 5 days.

In order to identify cells with statistically significant simultaneous activity ($p < 0.05$), we used an approach similar to the one proposed by Schwartz et. al. (Schwartz et al., 1998), by running 1000 Monte Carlo simulations based on the measured calcium transient frequency with uniform distribution (using a uniform time delay on each calcium trace as a null hypothesis of independent neural activations produced similar results). This method allowed one to distinguish cells with a high likelihood of being simultaneously active and cells without significant simultaneous activations. The pairwise asymmetric correlation coefficient was calculated as the average of the two asymmetric correlation coefficients between two neurons. For each cluster, the intra-cluster synchrony S was calculated as the average of the pairwise asymmetric correlation coefficients of neurons within the cluster. The intra-cluster synchrony change ΔS before and after cocaine injection was then calculated by $\Delta S = (S_2 - S_1)/ (S_2+S_1)$, where S_1 is the intra-cluster synchrony before cocaine injection and S_2 is the intra-cluster synchrony after cocaine injection. Similarly, the intra-cluster synchrony change before and after saline or between fine movement (FM) and ambulation (AM) states can be calculated. The inter-cluster synchrony X was calculated as the average of the pairwise asymmetric correlation coefficients of neurons in each cluster with the neurons from the other clusters. The inter-cluster synchrony change ΔX before and after cocaine injection was then calculated by $\Delta X = (X_2 - X_1)/ (X_2+X_1)$, where X_1 is the inter-cluster synchrony before cocaine injection and X_2 is the inter-cluster synchrony after cocaine injection. Similarly, the inter-cluster synchrony change before and after saline injection or between fine movement (FM) and ambulation (AM) states can be calculated. Similarly to the synchrony change, the cluster activity $\Delta F/F$ change ΔK before and after cocaine injection was calculated by $\Delta K = (K_2 - K_1)/ (K_2+K_1)$, where K_1 is the cluster $\Delta F/F$ before cocaine injection and K_2 is the cluster $\Delta F/F$ after cocaine injection. The cluster activity $\Delta F/F$ change before and after saline injection or between fine movement (FM) and ambulation (AM) states was calculated.

Definitions of Mouse Behavior

The behavioral analysis was performed using custom scripts in MATLAB. Based on the behavioral videos, the centroids of the mouse body were tracked (Ziv et al., 2013). Subsequently, the behavioral variables such as locomotion distance and velocity were calculated. The velocity data were smoothed by a moving average filter with a 0.5-second time window. We define six behavioral variables: ambulation, immobility, fine movement, motion initiation, motion termination, and maximum velocity. We followed the definition by Kravitz et. al. (Kravitz et al., 2010) for the calculation of ambulation, immobility, and fine movement. Ambulation was defined as the periods when the mouse's velocity is greater than 2 cm/s for at least 0.5 second. Immobility was defined as the periods when the mouse's velocity is less than 0.05 cm/s for at least 1 s. And movement that was not ambulation or immobility was defined as fine movement. For behavioral variable Ambulation, Immobility, and Fine movement, the binary behavior vectors were generated based on the behavior status (1 - yes, 0 - no). We defined two velocity thresholds: 0.2 cm/s and 2 cm/s. The motion initiation (MI) was defined as described by Polack et. al. (Polack et al., 2013), and was first identified by the time (T_1) at which the velocity crossed the second level of velocity threshold (2 cm/s) and remained greater than this threshold for at least 1 s, and then the motion initiation time onset was defined as the time (prior to T_1) at which the velocity reach the first threshold (0.2 cm/s). The motion termination (MT) was first identified as the time (T_2) at which mouse locomotion velocity from higher velocity crossed the higher threshold (2 cm/s) and remained below this level for at least one second, and then the motion termination time onset was defined as the

time (after T_2) at which the velocity reach the lower threshold (0.2 cm/s). The maximum velocity (V_{max}) onset time is the time at which there is a maximum velocity.

Neuronal activities for Different Behavioral Variables

For the behavior variables motion initiation, motion termination, and maximum velocity, the calcium activity and the locomotion velocity in the period of interest (from -4 s to +4 s relative to the behavior time onset) were extracted for all the neurons recorded from the D1-Cre and D2-Cre mice. For each mouse, the averaged activity of behavior variable MI, MT and V_{max} from all neurons and all periods of interert were calculated as $\Delta F/F_B = \Sigma_{m=1:M}\Sigma_{n=1:N}\Delta F/F(m,n)$, where B indicates behavior variable MI, MT or V_{Max}, M is the neuron number, N is the case number of behavior variable B and $\Delta F/F(m,n)$ is the calcium activity for neuron m in the n^{th} period of interest. So we calculated the the normalized calcium activity as $\Delta F/F_N = (\Delta F/F_B - \Delta F/F_{MIN})/(\Delta F/F_{MAX} - \Delta F/F_{MIN})$, where $\Delta F/F_{MAX} = \max\{\Delta F/F_{MI}, \Delta F/F_{MT}, \Delta F/F_{Vmax}\}$, and $\Delta F/F_{MIN} = \min\{\Delta F/F_{MI}, \Delta F/F_{MT}, \Delta F/F_{Vmax}\}$.

The average calcium activity during AM, IM and FM behavior were calculated by $\Delta F/F_B = (1/T_B)\Sigma_{t\in B}\Delta F/F(t)$, where B indicates AM, FM, or IM, T_B is the duration of behavior B. Thus the activity change by cocaine(or saline) injection can be calculated by $\Delta M = (\Delta F/F_{B2} - \Delta F/F_{B1})/(\Delta F/F_{B1} + \Delta F/F_{B2})$, where $\Delta F/F_{B1}$ is the average calcium activity before cocaine (or saline) injection and $\Delta F/F_{B2}$ is the average calcium activity after cocaine injection. Also, by dividing the velocity into different ranges we also calculated the mean neural activity, defined as the time averaged fluorescent change, at discrete steps as a function of velocity.

Correlation Analysis of Cluster Activities and Behavior Variables

Correlations were calculated between the locomotion velocity in the period of interest (V_{max}) and the averaged cluster fluorescent change (defined as the averaged $\Delta F/F$ of all neurons in each cluster). For the V_{max}, the behavioral vectors(B) were constructed as the locomotion velocity ranging from -4 s to +4 s relative to the V_{max} time onset as defined above. And the corresponding cluster fluorescent changes signal was extracted as the cluster vector (C). The cluster fluorescent changes in the immobility behavior were extracted as the baseline. A bootstrap resampling (n = 2000) was used to test the statistical significance of the fluorescent response relative to the baseline fluorescent changes. Only the significant cluster ($p < 0.05$) was kept for further correlation analysis. For each V_{max} time onset point, the sample cross correlation of behavioral vector and the cluster vector was calculated as the following (Chen et al., 2013a):
For data pair (B, C), an estimate of the lag k cross-covariance is

$$COV_{BC}(k) = \begin{cases} \frac{1}{n}\sum_{t=1}^{n-k}(B_t - \bar{B})(C_{t+k} - \bar{C}), & k = 0, 1, 2 \ldots \\ \frac{1}{n}\sum_{t=1}^{n-k}(C_t - \bar{C})(B_{t+k} - \bar{B}), & k = -1, -2 \ldots \end{cases}$$

where $\bar{B}$ and $\bar{C}$ are sample mean of behavioral vector and cluster vector. Thus an estimate of the sample cross correlation is calculated by:

$$\mathrm{R_{BC}}(k) = \frac{\mathrm{COV}_{BC}(k)}{\mathrm{COV}_{BB}(0)\mathrm{COV}_{CC}(0)}, \qquad k = 0, \pm 1, \pm 2 \ldots$$

Where $COV_{BB}(0)$ and $COV_{CC}(0)$ are the standard deviation of the behavioral vector and the cluster vector. For each sample cross correlation, the positive peak (R) represents the correlation between the cluster vector and behavioral vector. The statistical significance of the correlation R was determined by a permutation test as the following: Each data point along the cluster vector was randomly shuffled, and thus a distribution of 2000 correlation values R_{Rand} were generated by calculating the sample cross correlation between the behavioral vector and the randomly shuffled cluster vector. The p value for the significance of R was calculated as the fraction of the total number of R_{Rand} with the values greater than R. The data pair with $p < 0.05$ was denoted as correlated pair, otherwise denoted as uncorrelated pair. The cross correlation R of the uncorrelated pair was set to zero. For each cluster, a 2000-time bootstrap resampling was performed on all the data pairs to obtain the mean and the 95% confidence intervals of the cross correlation R. For each animal, the averaged cross correlation of all clusters was calculated. The averaged cross correlations of all the D1 and D2 mice for five days were calculated to show the reliability of the correlation between cluster activity and locomotion velocity.

The Clusters in Dorsomedial Striatum and Dorsolateral Striatum

To examine the differences in cluster activity and cluster synchrony changes between dorsomedial and dorsolateral striatum, we splitted the medial-lateral axis to three region, dorsomedial striatum (DMS), dorsolateral stiatum (DLS) and region between DMS and DLS (MIDDLE). The range of the cluster centroid in medial-lateral axis from all the mice was from –390 to 390 μm relative to the center of the field of view. So the clusters with centroid coordinates along the medial-lateral axis less than –130 μm was classified to DMS cluster, and clusters with centroid coordinates along the medial-lateral axis greater than 130 μm was classified to DLS cluster. The clusters with centroid coordinates along the medial-lateral axis between –130 μm and 130 μm was classified as MIDDLE cluster.

Behavior decoding analysis

Two types of decoding experiments, i.e., behavioral state decoding (binary variables) and velocity decoding (continuous variables), were conducted to determine if cluster activities, the randomly selected subset of single neurons,or population activities of D1-MSN and D2-MSN encode the behavioral relevant information. Machine learning algorithms were used for different decoding tasks.

Behavioral state decoding: We decoded four different behavioral states (AM, IM, FM and CO) based on (1) cluster activities (Clusters), (2) the activities of randomly selected subset of single neurons (Rand Neurons; the number of randomly selected neurons was equal to the number of clusters for each animal), and (3) population activities (Population) of D1-MSN and D2-MSN. We constructed a C5.0 decision tree classifier (Quinlan, 1986) for each behavioral state. Decoding performance was evaluated based on ten-fold cross-validation (Duda et al., 2000). The original sample is randomly partitioned into 10 equal sized subsamples. In each iteration, the C5.0 classifier was trained by 90% subset of the data (Clusters: $\{C_1,C_2,\ldots, C_i,\ldots,C_N; B_t\}_{Train}$, where C_i is the cluster ΔF/F of each mouse, N is the number of clusters, and B_t is the training behavior state vector; Rand Neurons: $\{RN_1,RN_2,\ldots, RN_i,\ldots, RN_N; B_t\}_{Train}$, where RN_i is the ΔF/F of the selected neuron of each mouse, N is the number of clusters, and B_t is the training behavior state vector; Population: $\{P; B_t\}_{Train}$, where P is the averaged ΔF/F from all neurons of each mouse, B_t is the training behavior state vector), and tested by the remaining 10% subset of data (Clusters: $\{C_1,C_2,\ldots,C_i,\ldots,C_N\}_{Test}$; Rand Neurons: $\{RN_1,RN_2,\ldots,RN_i,\ldots,RN_N\}_{Test}$; Population: P_{Test}). The decoding accuracy was calculated as the ratio of the number of corrected labeled cases to the total number of cases. To correct for imbalanced class distribution, we used the balanced accuracy(Brodersen et al., 2010). In Rand Neurons decoding experiments, decoding accuracy was calculated as the average of accuracies from 20 independent runs with different random combinations of randomly selected single neurons (Note: the number of randomly selected single neurons was equal to the number of clusters for each mouse, therefore the number of decoding inputs between cluster activities and randomly selected single neurons remained the same). The machine learning algorithm were implemented in an R package C50 (https://cran.r-project.org/). More details about the algorithm were described in previous study (Chen and Herskovits, 2010). For behavioral state AM, IM and FM, the dataset of the first three sessions in day one were used. For behavioral state CO, dataset of all six sessions in each day and all five days were used. In cluster decoding tasks, for each predictor, the receiver operating characteristic (ROC) curve analysis was conducted and the variable importance of each predictor was measured as the area under the ROC curve (Hanley and McNeil, 1982). The variable importance of cluster indicates the weighted contribution of each cluster in the decoding. Spearman rank correlation was used as the metric of the similarity for the variable importance for different behavior states (AM, IM, FM, and CO) decoding. The averaged similarity of the normal locomotion behavior state was calculated as the average of pairwise similarity {AM, FM}, {AM, IM}, and {FM, IM}. And the averaged similarity of the cocaine-locomotion behavior state was calculated as the average of pairwise similarity {CO, AM}, {CO, IM}, and {CO, FM}.

Velocity decoding: Gradient boosting machine, or GBM, (Friedman, 2002) algorithm were used for continuous velocity decoding. GBM was implemented in R with the gbm and plyr packages (https://cran.r-project.org/). GBM iteratively added basis functions in a greedy fashion to reduce the root mean square loss function. The base learner was a tree model and parameters were tuned by using internal cross-valdiation. Three decoding tasks were conducted by using cluster activity, the activities of randomly selected subset of single neurons (the number of randomly selected neurons equals to the number of clusters for each animal), and population activity to predict the locomotion velocity. Similar to the C5.0 classifier, the GBM model was evaluated using ten-folder cross-valifdation. The decoding performance was measured by the root mean square of error (RMSE). For each mouse, the first three sessions of dataset in day one were used in the velocity decoding tasks.

Statistics

All reported sample numbers represent biological replicates. All data were presented as mean ± sem unless otherwise stated. All statistical analyses were performed with Graphpad Prism (Graphpad) and Matlab (Mathworks). Mann Whitney test, Wilcoxon matched-pairs signed rank test, Pearson's correlation, Spearman's rank correlation, bootstrap resampling, random permutation and Monte Carlo simulations were used for statistical analysis.

Supplemental References

Arther, D.a.V., S. (2007). k-means++: The Advantages of Careful Seeding. In SODA '07 Proceedings of the eighteenth annual ACM-SIAM symposium on Discrete algorithms, pp. 1027-1035.

Brodersen, K.H., Ong, C.S., Stephan, K.E., and Buhmann, J.M. (2010). The Balanced Accuracy and Its Posterior Distribution. In Proceedings of the 2010 20th International Conference on Pattern Recognition (IEEE Computer Society), pp. 3121-3124.

Chen, J.L., Carta, S., Soldado-Magraner, J., Schneider, B.L., and Helmchen, F. (2013a). Behaviour-dependent recruitment of long-range projection neurons in somatosensory cortex. Nature 499, 336-340.
Chen, R., and Herskovits, E.H. (2010). Machine-learning techniques for building a diagnostic model for very mild dementia. NeuroImage 52, 234-244.

Chen, T.W., Wardill, T.J., Sun, Y., Pulver, S.R., Renninger, S.L., Baohan, A., Schreiter, E.R., Kerr, R.A., Orger, M.B., Jayaraman, V.*, et al.* (2013b). Ultrasensitive fluorescent proteins for imaging neuronal activity. Nature 499, 295-300.

Dombeck, D.A., Graziano, M.S., and Tank, D.W. (2009). Functional clustering of neurons in motor cortex determined by cellular resolution imaging in awake behaving mice. The Journal of neuroscience : the official journal of the Society for Neuroscience 29, 13751-13760.

Duda, R.O., Hart, P.E., and Stork, D.G. (2000). Pattern Classification (2nd Edition) (Wiley-Interscience).

Friedman, J.H. (2002). Stochastic gradient boosting. Comput Stat Data Anal 38, 367-378.
Hanley, J.A., and McNeil, B.J. (1982). The meaning and use of the area under a receiver operating characteristic (ROC) curve. Radiology 143, 29-36.

Kerlin, A.M., Andermann, M.L., Berezovskii, V.K., and Reid, R.C. (2010). Broadly tuned response properties of diverse inhibitory neuron subtypes in mouse visual cortex. Neuron 67, 858-871.
Kravitz, A.V., Freeze, B.S., Parker, P.R., Kay, K., Thwin, M.T., Deisseroth, K., and Kreitzer, A.C. (2010). Regulation of parkinsonian motor behaviours by optogenetic control of basal ganglia circuitry. Nature 466, 622-626.

Kuglin, C.D.a.H., D.C. (1975). The phase correlation image alignment method. In Proc Int Conf Cybernetics Society, pp. 163-165.

Lindeberg, T. (1998). Feature Detection with Automatic Scale Selection. International Journal of Computer Vision 30, 79-116.

Mukamel, E.A., Nimmerjahn, A., and Schnitzer, M.J. (2009). Automated analysis of cellular signals from large-scale calcium imaging data. Neuron 63, 747-760.

Ozden, I., Lee, H.M., Sullivan, M.R., and Wang, S.S. (2008). Identification and clustering of event patterns from in vivo multiphoton optical recordings of neuronal ensembles. Journal of neurophysiology 100, 495-503.

Pham, D.T., Dimov, S.S., Nguyen, C.D. (2005). Selection of K in K-means clustering. Proc IMechE 219, 103-119.

Pinto, L., and Dan, Y. (2015). Cell-Type-Specific Activity in Prefrontal Cortex during Goal-Directed Behavior. Neuron 87, 437-450.

Pnevmatikakis, E.A., Soudry, D., Gao, Y., Machado, T.A., Merel, J., Pfau, D., Reardon, T., Mu, Y., Lacefield, C., Yang, W.*, et al.* (2016). Simultaneous Denoising, Deconvolution, and Demixing of Calcium Imaging Data. Neuron 89, 285-299.

Polack, P.O., Friedman, J., and Golshani, P. (2013). Cellular mechanisms of brain state-dependent gain modulation in visual cortex. Nature neuroscience 16, 1331-1339.

Rand, W.M. (1971). Objective Criteria for the Evaluation of Clustering Methods. Journal of the American Statistical Association 66, 846-850.

Schwartz, T.H., Rabinowitz, D., Unni, V., Kumar, V.S., Smetters, D.K., Tsiola, A., and Yuste, R. (1998). Networks of coactive neurons in developing layer 1. Neuron 20, 541-552.

Vogelstein, J.T., Watson, B.O., Packer, A.M., Yuste, R., Jedynak, B., and Paninski, L. (2009). Spike inference from calcium imaging using sequential Monte Carlo methods. Biophysical journal 97, 636-655.

Ziv, Y., Burns, L.D., Cocker, E.D., Hamel, E.O., Ghosh, K.K., Kitch, L.J., El Gamal, A., and Schnitzer, M.J. (2013). Long-term dynamics of CA1 hippocampal place codes. Nature neuroscience 16, 264-266.